Title
Allosteric pathways in tetrahydrofolate sensing riboswitch with dynamics correlation network

Journal
Molecular Omics, 13(1)

ISSN
2515-4184

Authors
Zhang, Jin-Mai
Jiang, Cheng
Ye, Wei
et al.

Publication Date
2016-12-20

DOI
10.1039/c6mb00630b

Peer reviewed

HHS Public Access

Author manuscript

Mol Biosyst. Author manuscript; available in PMC 2017 December 20.

Published in final edited form as:

Mol Biosyst. 2016 December 20; 13(1): 156–164. doi:10.1039/c6mb00630b.

Allosteric Pathways in Tetrahydrofolate Sensing Riboswitch with Dynamics Correlation Network

Jin-Mai Zhang[1], **Cheng Jiang**[1], **Wei Ye**[1], **Ray Luo**[2,*], and **Hai-Feng Chen**[1,3,*]

[1]State Key Laboratory of Microbial metabolism, Department of Bioinformatics and Biostatistics, College of Life Sciences and Biotechnology, Shanghai Jiaotong University, 800 Dongchuan Road, Shanghai, 200240, China

[2]Departments of Molecular Biology and Biochemistry and Biomedical Engineering, University of California, Irvine, CA 92697-3900

[3]Shanghai Center for Bioinformation Technology, 1278 Keyuan Road, Shanghai, 200235, China

Abstract

Riboswitches are *cis*-acting genetic control elements. Due to their fundamental importance in bacteria gene regulation, riboswitches have been proposed as antibacterial drug targets. Tetrahydrofolate (THF) is an essential cofactor of one-carbon transfer reaction and downregulates the expression of downstream gene. However, the information how to transfer from the binding site of THF to the expression platform is still unsolved. Here, nucleotide/nucleotide dynamics correlation network based on all-atom molecular dynamic simulation was used to reveal the regulation mechanism of THF-sensing riboswitch. Shortest pathway analysis based on network illustrates that there is an allosteric pathway through P2 helix to pseudoknot, then to P1 helix in THF-riboswitch. Thus the hypothesis of "THF-binding induced allosteric switching" was proposed and valuated by THF and pseudoknot weakened experiments. Furthermore a possible allosteric pathway of C30-C31-G33-A34-G35-G36-G37-A38-G48-G47-U46-A90-U91-C92-G93-C94-G95-C96 was identified and confirmed by the perturbation of network. The proposed allosteric mechanism and the underlying allosteric pathway provide fundamental insights for the regulation of THF sensing riboswitch.

Keywords

THF; riboswitch; dynamics correlation network; Community; allosteric pathway

Introduction

Riboswitches are RNA structures which are found in most bacteria, plants and fungi.[1, 2] Since the first TPP riboswitch[3] was reported, more than 20 classes of riboswitches have been found until now.[4, 5] Riboswitches are typically located in the 5′-untranslated region (UTR) of mRNA and often conceptually split into two parts: the aptamer and the expression platform[6]. The aptamer domain binds the small molecule with high specificity and affinity,

*Corresponding authors: haifengchen@sjtu.edu.cn; rluo@uci.edu, Tel: 86-21-34204348, Fax: 86-21-34204348.

while the expression platform in turn supplies interfaces with many other gene expression apparatus[7]. Riboswitches can regulate the activity of mRNA in transcription and translation[8] levels just like regulatory ncRNAs[9] in eukaryotic. Tetrahydrofolate (THF) is the reductive form of folate and an essential cofactor of one-carbon transfer reaction.[10] Genes involved in the transportation and biosynthesis of folate and its derivatives are always controlled by the THF riboswitch.[11] In 2011, two groups reported two crystals about the THF riboswitch. Batey *et al* revealed that the riboswitch can bind two THF, one in the three-way junction another in the pseudoknot[12]. Patel *et al* revealed a single THF binding site in the three-way junction which was far away from the effective site.[13] It is well known that allostery is a fundamental regulatory strategy adopted by many proteins and nucleic acids[14, 15], which modulates the function and adaptability sensitively. Allosteric macromolecules always contain at least two functional active sites: the effector binding site and the catalytic site.[16]

In order to reveal the regulation mechanism of THF riboswitch, single THF binding site system was used in this research. The THF riboswitch structure is shown in Figure 1A. The riboswitch consists of four helices (P1, P2, P3, P4), five joining regions (J1/2, J2/1, J2/3, J3/4, J4/2), and two hairpin loops (L3, L4). Helix P1 consists of G1–G6 and C96-U100, helix P2 with G11–G20 and U78-C87, helix P3 with G29–G36 and C50-A57, helix P4 with C62-G73, junction J1-2/J2-1 from A7 to A10 and G88 to G95, junction J2-3/J3-4/J4-2 from C21 to U28, C58-A61 and G74–G77. THF binds to helix P3 near J2/3. Helix P3 plays crucial role in locking ligand and sequestering the ribosome binding site.

It is still unclear how THF riboswitch downregulates the gene expression. In this study, we intend to discover regulatory pathway and mechanism of THF riboswitch by answering the following two questions. (1) Is there an allosteric regulation for THF riboswitch? (2) If so, what are the allosteric pathways that connect the THF binding site and the regulating site? In order to answer these questions, community network analysis [17] based on all-atom MD simulations was utilized to address each of these issues. Overall, these studies show the feasibility of using MD to understand riboswitch function and provide an opportunity to look for common themes in ligand binding and conformational dynamics.

Dynamic network analysis, which has been previously used to illustrate the allosteric phenomenon of aminoacyl-tRNA synthetase, was employed to elucidate the allosteric pathways of THF sensing riboswitch.[18] The pathway shows that P3 helix and pseudoknot[19] play key roles in information transfer. Mutants of G41U and G41A-G42U-U91A from pseudoknot confirmed that pseudoknot can stabilize the base pairs of P1 helix. From the comparisons of the networks between free and bound riboswitch, the allosteric pathway and key bases were proposed for transferring the regulation information from the THF allosteric sites to the expression platform. The process based on allosteric pathway might improve the regulation efficiency for downstream gene. **(Reference)

Materials and Method

Molecular dynamics simulations

The structures of free (pdb code: 3SUY) and THF bound riboswitches (pdb code: 3SUX) were downloaded from RCSB.[13] All structural visualizations were conducted in PyMOL

1.5.03. AMBER12 was used to perform efficient simulations with periodic boundary conditions. Hydrogen atoms were added using the LEaP module of AMBER12. Counter-ions were added to maintain system neutrality. All systems were solvated in a truncated octahedron box of TIP3P waters with a buffer of 10 Å. The pairwise interactions (van der Waals and direct Coulomb) were computed with a default cutoff distance of 8 Å. Particle Mesh Ewald (PME) was employed to treat long-range electrostatic interactions in AMBER12[20]. The improved ff99SBildn[21] force field was used for the intramolecular interactions. In order to compare the performance of different force fields, ff99bsc0 was also used in this study for bound riboswitch. ** The SHAKE algorithm[22] was used to constrain bonds involving hydrogen atoms. All MD simulations were accelerated with the CUDA version of PMEMD in GPU cores of NVIDIA® Tesla K20. Up to 10000-step steepest descent minimization was performed to relieve any structural clash in the solvated systems. This was followed by a 400-ps' heating up and a 200-ps' equilibration in the NVT ensemble at 298K. The Langevin thermostat was used in the preparation runs with a friction constant of 1 ps-1 and the Berendsen thermostat with default setting was used in the production runs.

To compare the difference between free and bound riboswitches, four independent trajectories of 100 ns each were simulated. 1 μs trajectories in all were collected for the wild type and mutant systems at 298K, taking about 1200 GPU hours. Detailed simulation conditions are listed in Table 1.

Data analyses

RMSD and RMSF were calculated and analyzed to monitor the convergence of system and the relative variation of nucleotides. PCA were used to monitor the motion mode of nucleotides. Hydrophobic contacts, electrostatic (i.e. charge-charge) interactions and hydrogen bonds were used to identify the intramolecular interaction between THF and riboswitch. Hydrogen bond is defined that the distance between two polar heavy atoms either with a hydrogen atom is less than 3.5 Å. For each simulation, sampling was conducted every 10 ps (10000 snapshots for 100 ns' simulations). These interactions were handled with in-house software. All pictures are plotted with Origin 9.1.

Dynamics Network Analyses

Every nucleotide was divided into two nodes (backbone and base) for more detailed analysis of their fluctuation dynamics. The fluctuation correlation between any pair of nodes was calculated as

$$C_{ij}=\frac{\langle \Delta \vec{r_i}(t) \cdot \Delta \vec{r_j}(t) \rangle}{\sqrt{(\langle \Delta \vec{r_i}(t)^2 \rangle \langle \Delta \vec{r_j}(t)^2 \rangle)}}$$

where $\Delta \vec{r_i}(t)=\vec{r_i}(t)-\langle \vec{r_i}(t) \rangle$, $\vec{r_i}(t)$ is the position of node i at time t, and $\langle \cdot \rangle$ represents a time averaging. These elements were conveniently organized as a covariance matrix for a simulated system. In the current study, the covariance matrix for each system was constructed using snapshots (every 2 ps) in the last 50 ns of all simulated trajectories.

Besides nodes, “edge” that transfers allosteric information from one node to another is also a key concept in network construction. An edge is defined between any two nodes without covalent bond but with heavy atoms closer than 4.5 Å over 75% sampling time. The strength of the edge is defined as the absolute value of the inter-node correlation (C_{ij}) between node i and j. The number of connected edges at each node is defined as the degree of the node. Correlation-weighted degree, which is the summation of strengths of all edges connected to a given node, indicates the importance of the node. After the network construction, network topological analyses were performed using Cytoscape3.2.0[23]. The Floyd-Warshall algorithm was used to calculate the shortest path between any two nodes in the network[24]. For Community analyses, Girvan-Newman algorithm was utilized with the network tools developed by Luthey-Schulten Group[18, 24] and the strategy of process was successfully used in the allostery of riboswitch and protein[25, 26].

Results

THF stabilizing P1 helix of riboswitch

The Cα RMSDs of THF free and bound riboswitches are shown in supplementary Figure S1. This figure indicates that 100ns simulations are sufficient for the equilibration of these systems. The RMSF of THF free and bound riboswitches are shown in Figure 2. This figure shows that the fluctuation of bound riboswitch is significant lower than that of free riboswitch, especially on the regions of P1 helix (1–6, 90–100) and P2 helix (40–50). This shows that the binding of THF can stabilize the P1 and P2 helicies.

In order to further evaluate the conformational adjustment of riboswitch, pairwise C5′ distance difference between THF bound and free riboswitches was measured. Figure 3 illustrates the conformational adjustment of riboswitch upon the binding of THF. Green regions represent negative differences, indicating more compact structure, while red and blue regions indicate C5′ atoms pushed further away (more extended structure). In this figure, red and blue regions are located at nucleotides 90–100 and 38–43, suggesting that P1 helix and pseudoknot move further away from the main domain upon the disassociation of THF. Consistent observations are also found in the principal component analysis (PCA) as to be discussed below.

Distance different landscape indicates that P1 helix undergoes significant conformational changes for THF free riboswitch. To quantitatively identify the motion mode for conformational adjustment, PCA was carried out on THF bound and free systems. Overall the three most dominant components (named PC1, PC2, and PC3) represent most of the overall fluctuations. To clearly display the motion of P1 helix, structural projections along the first principal component (~40%) are shown in Figure 4. For the THF free riboswitch, P1 helix is in the opening and closing motion. Pseudoknot L3 also has the motion of far away from P1 helix. However, the THF bound riboswitch has no significant conformational changes. This indicates that P1 helix was stabilized by THF binding.

The alignment of average structures between THF bound and free riboswitch is shown in Figure 5. The most significant difference was found at the regions of P1 helix and pseudoknot. In order to more clearly highlight this difference, the distances between G6 and

C96, between A7 and G95 at P1 helix are shown in Figures 5B and 5C. The distance between G6 and C96 for free riboswitch is about 33 Å and 18Å for bound riboswitch. The distance between A7 and G95 is about 30 Å for THF free riboswitch and 16Å for THF bound riboswitch. These results also clearly indicate that P1 helix has significant opening propensity upon the disassociation of THF.

The previous work suggests that the P1 helix will sequester the ribosome binding site (RBS) and down-regulate the production of proteins involving folate synthesis and transportation[13]. Furthermore, the P1 helix is about 50Å away from the THF binding site. Therefore, this might be an allosteric regulation in this system.

Different Correlation Networks for THF Free and Bound Riboswitches

Structural analysis suggests that allosteric regulation may exist in the THF bound riboswitch. In order to reveal the allosteric molecular mechanism, dynamics network was used to analyze the nucleotide fluctuation correlation. To construct the correlation network, the covariance matrices were first calculated for the riboswitch. The dynamics cross-correlation maps (DCCMs) for THF free and bound riboswitches are shown Figure 6. Positive and negative correlations are shown in the upper and lower traiangles of the DCCM, respectively. This figure indicates that the correlations between P3 and P1 are much lower in the THF bound state than those in the THF free state. These regions are more compact in the THF bound state. The correlation difference between THF bound and free is mainly focused on P3 and P1 helicies. This demonstrates that the P3 helix is strongly correlated with P1 upon the THF binding.

Based on the covariance matrices, dynamics networks were constructed. The topology parameters of THF bound and free networks are listed in Table 2. The network centralization of the THF bound state is higher than that of the free state. The dynamics networks for THF free and bound states are shown in Figure 7. The number of nodes with weighted degree higher than five is 32 for THF bound state and more than that of THF free state (28). These important hub nodes might play key roles in the network, such as G27, U28, C30, C51, G48, G37, G98, and other nodes. Furthermore, six bases such as G37, A38, C39, C39, G41, G48, and U49 belong to the pseudoknot of THF bound riboswitch. Interestingly, the degrees of G98, G95, C50, C51, and C75 significantly decrease upon the dissociation of THF. For the whole network, the THF free network splits into two pieces. The information flow could not transfer from the allosteric site to P1 helix.

Different Communities for Different Networks

Dynamics correlation network shows that the networks are significantly different between THF bound and free riboswitches. To reveal the information transfer pathway, the Girvan-Newman algorithm was used to split the network into communities. The community network is shown in Figure 8, which shows that the THF bound network is clustered into seven connective communities. The information flow can freely transfer from the binding pocket of THF to the expression platform of P1 helix. However, the community network is significantly changed and P1 helix and L3 loop are isolated from the main community for the THF free state. Information flow can hardly transfer from the binding site to the

expression platform. These results are in agreement with those of the dynamics network analysis (shown in Figure 7). Note too that the information intensity of the bound community network is also stronger than that of the free community network, especially for the community of the binding pocket. Moreover, structural analysis indicates that there are two hydrogen bonds, four hydrophobic interactions, and eight electrostatic interactions between THF and riboswitch, with population higher than 50% (shown in Figure 9). These results indicate fairly strong binding interactions. Therefore a hypothesis of "binding induced allosteric switching" can be used to explain the regulation mode for THF riboswitch.

Validation of Hypothesis by Network Modification

In order to validate the above hypothesis, network modification to weaken the interactions between THF and riboswitch was used to study the effects on the community networks. This perturbation just deleted the edges between THF and riboswitch nodes in the network. The community network of weakened system is shown in Figure 10. The number of community for weakening operation did not change, however the nucleotides within different communities were rearranged. In summary this modification leads to significant repartition of the community network. This finding confirms that the interactions between THF and riboswitch indeed influence the community network and further support our hypothesis of binding induced allosteric switching mechanism.

Validation of Hypothesis by Pseudoknot Weaken

Pseudoknots are essential for various cellular activities by forming integral parts of the RNA structures [27–29]. The previous works confirm that pseudoknot forms key tertiary pairs in ydao-riboswitch [30, 31]. Furthermore, the community of L3 pseudoknot was between P1 helix and P3 helix and played a key role in information transfer. To further evaluate the hypothesis of "binding induced allosteric switching", the communities of weaken pseudoknot for G41/G95 and G41/G42/G95 are constructed and shown in Figure 11. This figure indicates that P1 helix was splitted into one isolated community and has not information exchange with L3 and main part for weaken G41/G95 and G41/G42/G95. Therefore, weaken pseudoknot significant changed the correlation community and confirmed the hypothesis.

THF Allosteric Pathway

The network and community analyses of the wild type and mutants confirm that the THF binding induces allostery of riboswitch. Next, it is natural to identify the allosteric pathway based on the shortest path analysis between the allosteric site and the expression platform of P1 helix. One pathway was identified in the THF bound riboswitch: C30-C31-G33-A34-G35-G36-G37-A38-G48-G47-U46-A90-U91-C92-G93-C94-G95-C96 (Figure 12). However, we could not find a similar pathway in the THF free riboswitch. This indicates that these nucleotides are key nodes for information transfer in the THF bound riboswitch.

In order to further verify the allosteric pathway, network perturbation was used to study the effect of G48, which is the linkage node between P3 helix and L3 junction, the bottleneck of information transfer. Without carrying out another MD simulation, the perturbation was realized by weakening the edges between G48 and any nucleotide in the network. The

community network is shown in Figure 12B. There are 14 communities and more than those (11) of THF bound system. These communities are significantly repartitioned. This weakening process decreases the effectiveness of information transfer, confirming that G48 plays a key role in this allosteric switch.

Discussion

Comparison with Previous Works

The crystal structure shows that U28 and C58 can form stable hydrogen bonds with pterin of THF.[13] Two stable hydrogen bonds for U28/THF and C58/THF were found in the room-temperature MD simulations. These results are in good agreement with the structural analysis that THF forms important interactions with the riboswitch. The experimental data also indicate that the triple stacks of G29-THF-G59 can stabilize the binding pocket, which is consistent with our simulations that THF can form stable hydrophobic interactions with G29 and G59 (Figure 9). The previous experiment also suggests that pseudoknot interactions can stabilize helix P1.[13] The networks and communities of pseudoknot mutants suggest that the information flow fails to transfer within the riboswitch. This indicates that pseudoknot play an essential role in information transfer. This is consistent with the experimental observation.

Conclusion

Dynamics correlation network was used to research the allosteric mechanism of THF riboswitch. The results suggest that the correlation network of the THF bound riboswitch has more hub nodes than that of the THF free state. The community network of the bound state is clustered into a union community. However, the P1 helix and L3 junction are isolated from the community upon dissociation from THF. The information flow can freely transfer from the binding pocket of THF to the expression platform of the P1 helix. On the contrary, information flow can hardly transfer from the J2/3/4 junction to the expression platform in the THF free state. Therefore, a hypothesis of “THF-binding induced allosteric switching” is used to explain the THF binding and switch regulation. These observations were further confirmed with the results from community analysis based on the Girvan-Newman algorithm for pseudoknot and THF weakened networks. Finally, a possible allosteric pathway of C30-C31-G33-A34-G35-G36-G37-A38-G48-G47-U46-A90-U91-C92-G93-C94-G95-C96 is also identified based on the analysis of the network for the THF bound state and confirmed by network perturbation. Interestingly, no pathways could be found in the THF free state.

Acknowledgments

This work was supported by Center for HPC at Shanghai Jiao Tong University, the National High-tech R&D Program of China (863 Program) (2014AA021502), the National Natural Science Foundation of China (31620103901 and J1210047), Medical Engineering Cross Fund of Shanghai Jiaotong University (YG2013MS68, YG2014MS47, and YG2015MS56), and National Institutes of Health/NIGMS (GM093040 & GM079383).

References

1. Lee ER, Baker JL, Weinberg Z, Sudarsan N, Breaker RR. An allosteric self-splicing ribozyme triggered by a bacterial second messenger. Science. 2010; 329:845–8. [PubMed: 20705859]
2. Nguyen GT, Scaife MA, Helliwell KE, Smith AG. Role of riboswitches in gene regulation and their potential for algal biotechnology. J Phycol. 2016
3. Haller A, Altman RB, Souliere MF, Blanchard SC, Micura R. Folding and ligand recognition of the TPP riboswitch aptamer at single-molecule resolution. Proc Natl Acad Sci USA. 2013; 110:4188–93. [PubMed: 23440214]
4. Roth A, Breaker RR. The structural and functional diversity of metabolite-binding riboswitches. Annual review of biochemistry. 2009; 78:305–34.
5. Winkler W, Nahvi A, Breaker RR. Thiamine derivatives bind messenger RNAs directly to regulate bacterial gene expression. Nature. 2002; 419:952–6. [PubMed: 12410317]
6. Smith KD, Lipchock SV, Ames TD, Wang J, Breaker RR, Strobel SA. Structural basis of ligand binding by a c-di-GMP riboswitch. Nat Struct Mol Biol. 2009; 16:1218–23. [PubMed: 19898477]
7. Regulski EE, Moy RH, Weinberg Z, Barrick JE, Yao Z, Ruzzo WL, Breaker RR. A widespread riboswitch candidate that controls bacterial genes involved in molybdenum cofactor and tungsten cofactor metabolism. Mol Microbiol. 2008; 68:918–32. [PubMed: 18363797]
8. Serganov A, Yuan YR, Pikovskaya O, Polonskaia A, Malinina L, Phan AT, Hobartner C, Micura R, Breaker RR, Patel DJ. Structural basis for discriminative regulation of gene expression by adenine- and guanine-sensing mRNAs. Chem Biol. 2004; 11:1729–41. [PubMed: 15610857]
9. Holoch D, Moazed D. RNA-mediated epigenetic regulation of gene expression. Nat Rev Genet. 2015; 16:71–84. [PubMed: 25554358]
10. de Crecy-Lagard V, El Yacoubi B, de la Garza RD, Noiriel A, Hanson AD. Comparative genomics of bacterial and plant folate synthesis and salvage: predictions and validations. BMC genomics. 2007; 8:245. [PubMed: 17645794]
11. Ames TD, Rodionov DA, Weinberg Z, Breaker RR. A eubacterial riboswitch class that senses the coenzyme tetrahydrofolate. Chemistry & biology. 2010; 17:681–5. [PubMed: 20659680]
12. Trausch JJ, Ceres P, Reyes FE, Batey RT. The structure of a tetrahydrofolate-sensing riboswitch reveals two ligand binding sites in a single aptamer. Structure. 2011; 19:1413–23. [PubMed: 21906956]
13. Huang L, Ishibe-Murakami S, Patel DJ, Serganov A. Long-range pseudoknot interactions dictate the regulatory response in the tetrahydrofolate riboswitch. Proc Natl Acad Sci USA. 2011; 108:14801–6. [PubMed: 21873197]
14. Wootten D, Christopoulos A, Sexton PM. Emerging paradigms in GPCR allostery: implications for drug discovery. Nat Rev Drug Discov. 2013; 12:630–44. [PubMed: 23903222]
15. Penchovsky R, Breaker RR. Computational design and experimental validation of oligonucleotide-sensing allosteric ribozymes. Nat Biotechnol. 2005; 23:1424–33. [PubMed: 16244657]
16. Rivalta I, Sultan MM, Lee NS, Manley GA, Loria JP, Batista VS. Allosteric pathways in imidazole glycerol phosphate synthase. Proc Natl Acad Sci USA. 2012; 109:E1428–36. [PubMed: 22586084]
17. Girvan M, Newman ME. Community structure in social and biological networks. Proc Natl Acad Sci USA. 2002; 99:7821–6. [PubMed: 12060727]
18. Sethi A, Eargle J, Black AA, Luthey-Schulten Z. Dynamical networks in tRNA:protein complexes. Proc Natl Acad Sci USA. 2009; 106:6620–5. [PubMed: 19351898]
19. Puglisi JD, Wyatt JR, Tinoco I Jr. A pseudoknotted RNA oligonucleotide. Nature. 1988; 331:283–6. [PubMed: 3336440]
20. Case DA, Cheatham TE 3rd, Darden T, Gohlke H, Luo R, Merz KM Jr, Onufriev A, Simmerling C, Wang B, Woods RJ. The Amber biomolecular simulation programs. J Comput Chem. 2005; 26:1668–88. [PubMed: 16200636]
21. Ye W, Ji D, Wang W, Luo R, Chen HF. Test and Evaluation of ff99IDPs Force Field for Intrinsically Disordered Proteins. J Chem Inf Model. 2015; 55:1021–9. [PubMed: 25919886]

22. Ruymgaart AP, Cardenas AE, Elber R. MOIL-opt: Energy-Conserving Molecular Dynamics on a GPU/CPU system. J Chem Theory Comput. 2011; 7:3072–3082. [PubMed: 22328867]
23. Brohee S, Faust K, Lima-Mendez G, Vanderstocken G, van Helden J. Network Analysis Tools: from biological networks to clusters and pathways. Nat Protoc. 2008; 3:1616–29. [PubMed: 18802442]
24. del Sol A, Fujihashi H, Amoros D, Nussinov R. Residues crucial for maintaining short paths in network communication mediate signaling in proteins. Mol Syst Biol. 2006; 2 2006 0019.
25. Yang J, Liu H, Liu X, Gu C, Luo R, Chen HF. Synergistic Allosteric Mechanism of Fructose-1,6-bisphosphate and Serine for Pyruvate Kinase M2 via Dynamics Fluctuation Network Analysis. Journal of chemical information and modeling. 2016; 56:1184–92. [PubMed: 27227511]
26. Wang W, Jiang C, Zhang J, Ye W, Luo R, Chen HF. Dynamics Correlation Network for Allosteric Switching of PreQ1 Riboswitch. Scientific Reports. 2016
27. Peselis A, Serganov A. Structure and function of pseudoknots involved in gene expression control. Wiley Interdiscip Rev RNA. 2014; 5:803–22. [PubMed: 25044223]
28. Kang M, Eichhorn CD, Feigon J. Structural determinants for ligand capture by a class II preQ1 riboswitch. Proc Natl Acad Sci USA. 2014; 111:E663–71. [PubMed: 24469808]
29. Santner T, Rieder U, Kreutz C, Micura R. Pseudoknot preorganization of the preQ1 class I riboswitch. J Am Chem Soc. 2012; 134:11928–31. [PubMed: 22775200]
30. Ren A, Patel DJ. c-di-AMP binds the ydaO riboswitch in two pseudo-symmetry-related pockets. Nat Chem Biol. 2014; 10:780–6. [PubMed: 25086509]
31. Wilkinson SR, Been MD. A pseudoknot in the 3′ non-core region of the glmS ribozyme enhances self-cleavage activity. RNA. 2005; 11:1788–94. [PubMed: 16314452]

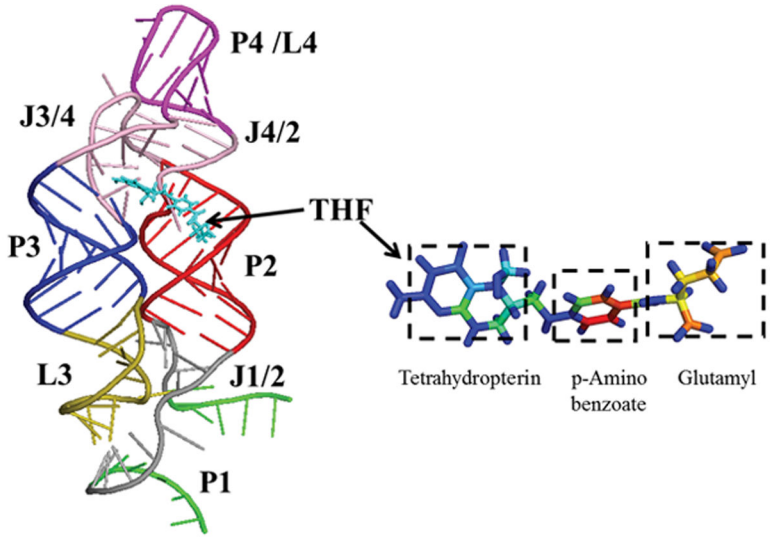

Figure 1.

Ribbon representation of the NMR structure for the THF riboswitch and THF. Helices P1, P2, P3, and P4 (green, brown, blue, and purple), junctions J1/2 and J2/3/4 (gray and pink), hairpin loops L3 and L4 (yellow-green and purple), THF (cyan) are labeled.

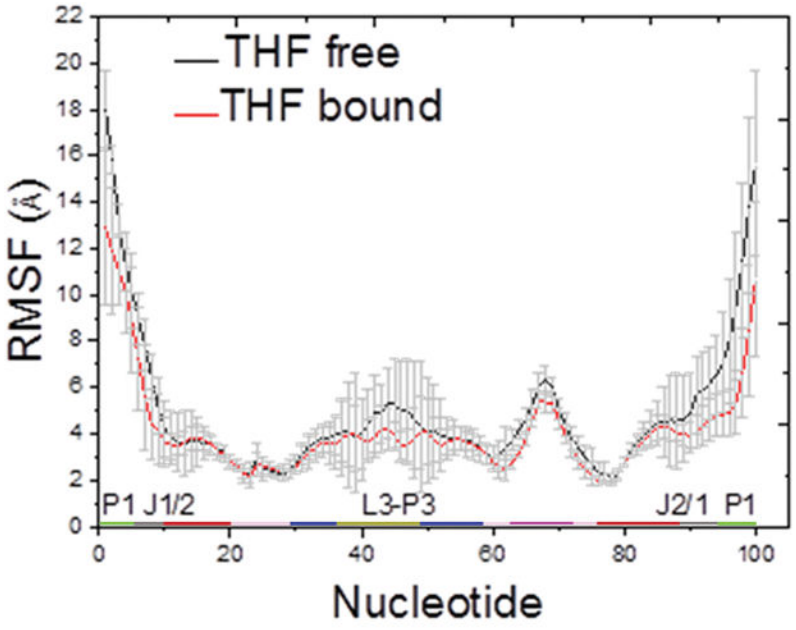

Figure 2.
C5′ RMSF for THF bound and free states.

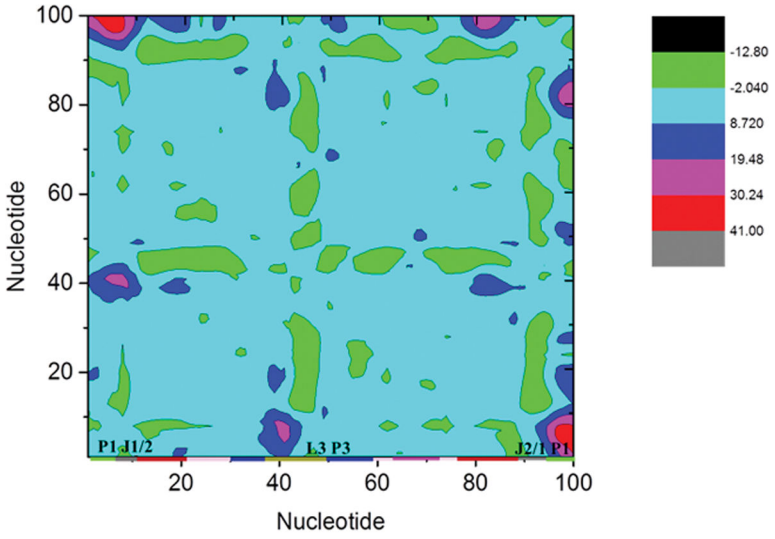

Figure 3.

Distance different landscape between THF bound and free states. Green regions represent negative differences, red and blue regions for positive differences.

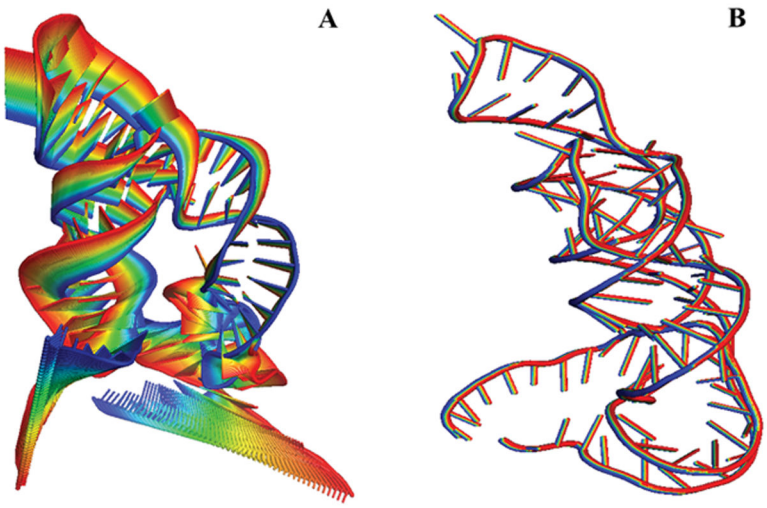

Figure 4.
Motion mode of PCA analysis for THF bound and free states. A: THF free state. B: THF bound state.

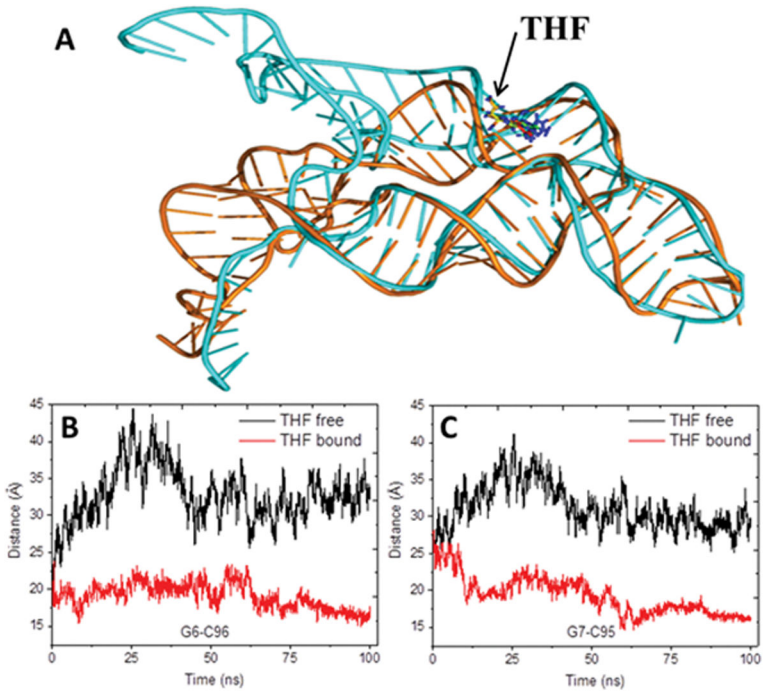

Figure 5.

The alignment of average structures for THF free and bound riboswitch and distance for two pairs of terminus base. A: alignment of average structures. Cyan represents THF free riboswitch, orange for bound riboswitch. B: Distances between G6-C96. C: distance between G7 and G95.

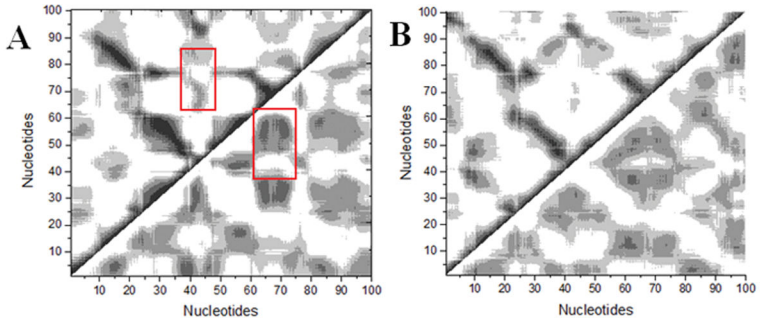

Figure 6.

DCCMs for THF bound and free states. A: THF bound. B: THF free. The strong (Cij = ±0.5–1.0), and weak (Cij = ±0.2–0.5) are represented by black and gray, respectively. The lower and upper triangles correspond to negative and positive correlations, respectively.

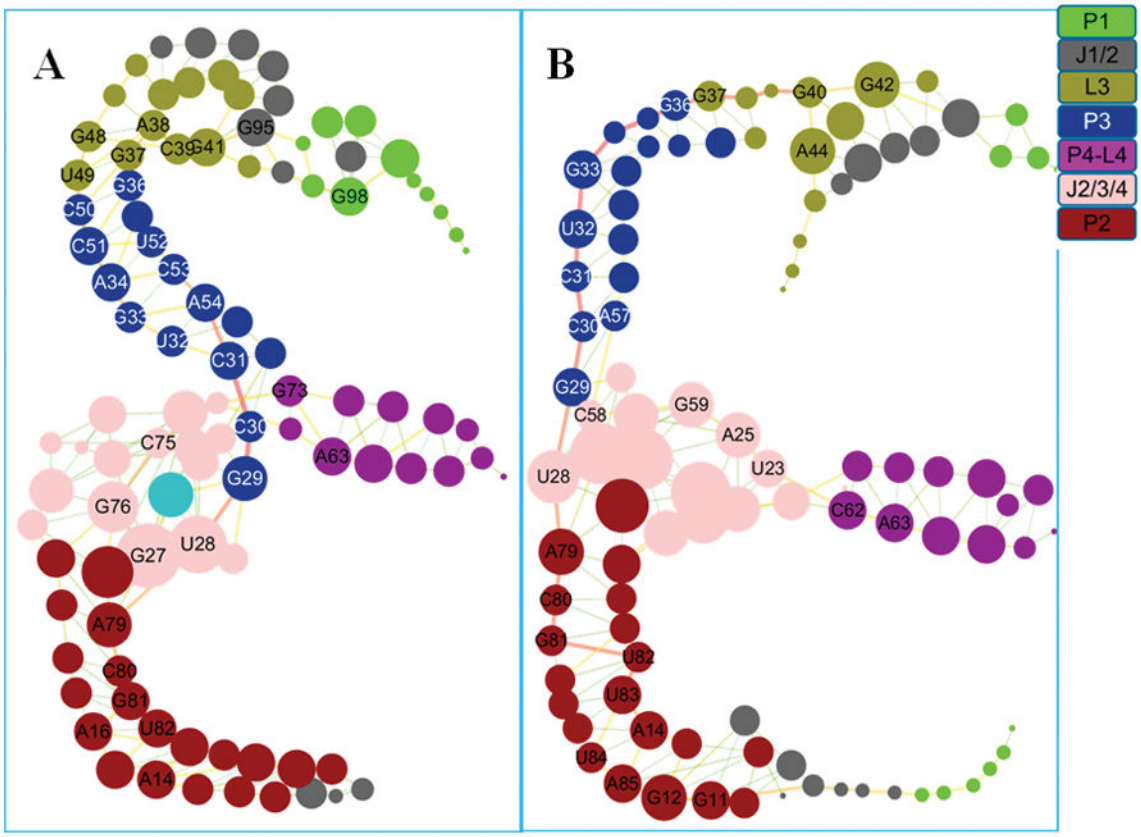

Figure 7.

Dynamics correlation networks for THF bound and free riboswitches. A: THF bound riboswitch. B: THF free riboswitch. Nodes are drawn to sizes based on the actual values for degree and are colored according to their structural domains. See labels in the coloring legend. Hub nodes with degree higher than 5 are labeled with the bases.

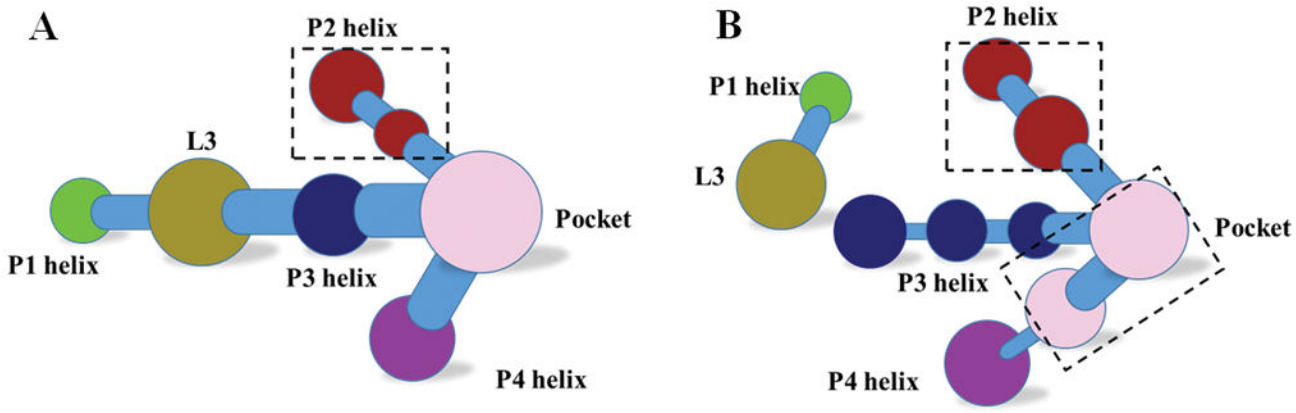

Figure 8.
Community networks for THF bound and free states. A: THF bound. B: THF free.

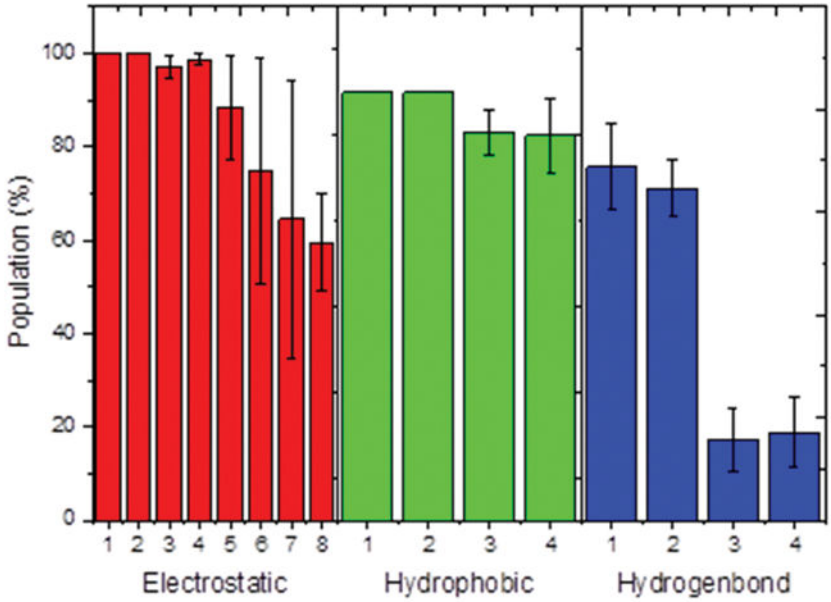

Figure 9.

Interactions between THF and riboswitch. Electrostatic interaction, 1:G59/THF,2:G77/THF, 3:G29/THF,4:A60/THF,5:C30/THF,6:A26/THF,7:U28/THF,8:G27/THF; Hydrophobic interaction, 1:U28/THF, 2:G29/THF, 3:C58/THF, 4:G59/THF; Hydrogen bond, 1:U28/THF, 2:C58/THF, 3:G77/THF, 4:G29/THF.

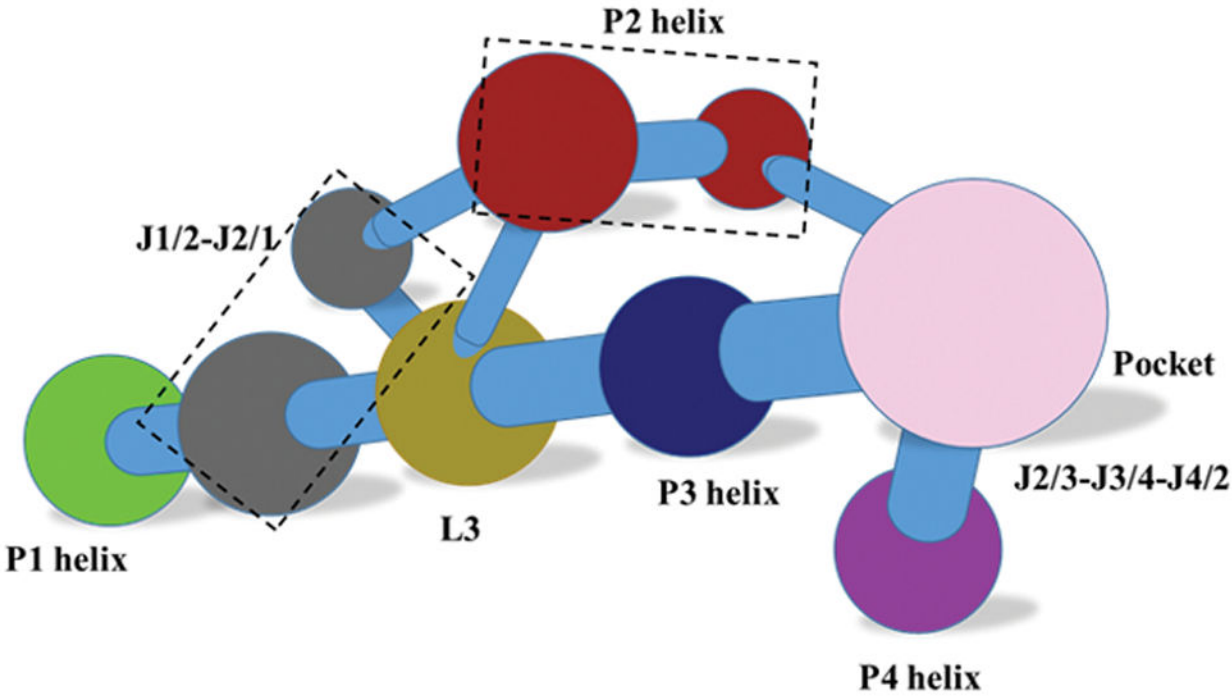

Figure 10.
Community network for THF weaken system.

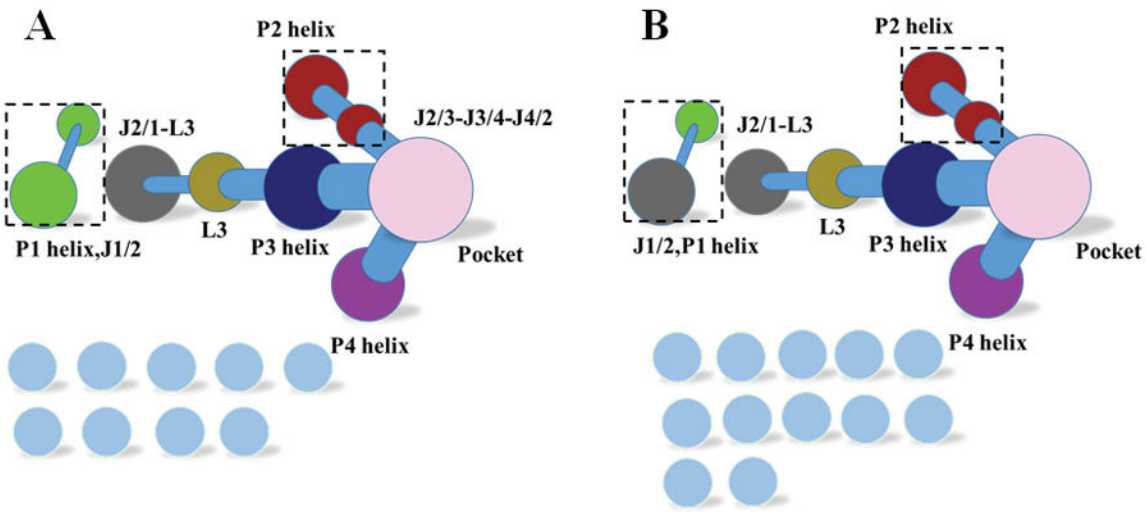

Figure 11.

Community network for weaken pseudoknot. A: G41/G95 weaken. B: G41/G42/G95 weaken.

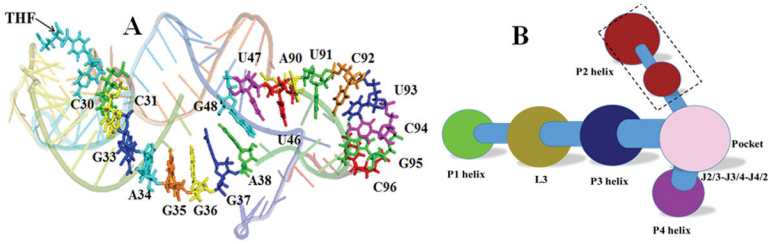

Figure 12.

Allosteric pathway and community network for weaken system. A: Allosteric pathway. B: Community network for G48 weaken.

Table 1

Simulation conditions for all systems.

System	Temperature(K)	Time(ns)	Traj. No.	Ions	Waters	Force Field
THF bound	**298K**	**100ns**	**4**	**101**	**104487**	**ff99SBildn**
THF bound	**298K**	**100ns**	**1**	**101**	**104487**	**ff99BSC0**
THF free	**298K**	**100ns**	**4**	**100**	**111761**	**ff99SBildn**

Table 2

Topology parameters of THF bound and free networks

System	Clustering coefficient	Network density	Network centralization	Network heterogeneity	Avg. number of neighbors
THF bound	0.503	0.042	0.050	0.303	4.16
THF free	0.428	0.041	0.042	0.39	4.00